Continuous, Highly Flexible, and Transparent Graphene Films by Chemical Vapor Deposition for Organic Photovoltaics

Lewis Gomez De Arco,[†,‡,§] Yi Zhang,[†,‡,§] Cody W. Schlenker,[‡] Koungmin Ryu,[†] Mark E. Thompson,[‡] and Chongwu Zhou[†,*]

[†]Department of Electrical Engineering and [‡]Department of Chemistry, University of Southern California, Los Angeles, California 90089. [§]These authors contributed equally.

ABSTRACT We report the implementation of continuous, highly flexible, and transparent graphene films obtained by chemical vapor deposition (CVD) as transparent conductive electrodes (TCE) in organic photovoltaic cells. Graphene films were synthesized by CVD, transferred to transparent substrates, and evaluated in organic solar cell heterojunctions (TCE/poly-3,4-ethylenedioxythiophene:poly styrenesulfonate (PEDOT:PSS)/copper phthalocyanine/fullerene/bathocuproine/aluminum). Key to our success is the continuous nature of the CVD graphene films, which led to minimal surface roughness (~0.9 nm) and offered sheet resistance down to 230 Ω/sq (at 72% transparency), much lower than stacked graphene flakes at similar transparency. In addition, solar cells with CVD graphene and indium tin oxide (ITO) electrodes were fabricated side-by-side on flexible polyethylene terephthalate (PET) substrates and were confirmed to offer comparable performance, with power conversion efficiencies (η) of 1.18 and 1.27%, respectively. Furthermore, CVD graphene solar cells demonstrated outstanding capability to operate under bending conditions up to 138°, whereas the ITO-based devices displayed cracks and irreversible failure under bending of 60°. Our work indicates the great potential of CVD graphene films for flexible photovoltaic applications.

KEYWORDS: graphene · chemical vapor deposition · transparent conductor · flexible photovoltaics · flexible solar cell · organic photovoltaics · transparent electrode

Solar energy harvesting using organic photovoltaic (OPV) cells has been proposed as a means to achieve low-cost energy due to their ease of manufacture, light weight, and compatibility with flexible substrates.[1] A critical aspect of this type of optoelectronic device is the transparent conductive electrode through which light couples into the device. Conventional OPVs typically use transparent indium tin oxide (ITO) or fluorine-doped tin oxide (FTO) as such electrodes.[1,2] However, the scarcity of indium reserves, intensive processing requirements, and highly brittle nature of metal oxides[3−5] impose serious limitations on the use of these materials for applications where cost, physical conformation, and mechanical flexibility are important.

Carbon nanotubes[6−8] and nanowires[9,10] have been used as alternative materials for electrodes in OPVs, but the roughness of such films was comparable to or larger than a typical device thickness, which may lead to significant shunt losses. In contrast, graphene is a one-atom thick, two-dimensional crystalline arrangement of carbon atoms with a quasi-linear dispersion relation and predicted mobility on the order of 10^6 $cm^2/V \cdot s$ for a charge carrier concentration $n_i \sim 10^{12}$ cm^{-2}.[11] Graphene monolayer has a transparency of 97−98%,[12] and the sheet resistance of undoped graphene is on the order of ~6 kΩ.[13−16] Graphene films are suitable for applications as transparent conductive electrodes where low sheet resistance and high optical transparency are essential. Conventional methods to obtain graphene thin films such as epitaxial growth,[17] micromechanical exfoliation of graphite,[18] and exfoliation of chemically oxidized graphite[19,20] are either expensive, unscalable, or yield graphene with limited conductivity due to a high defect density. Recently, graphene films obtained from reduced graphene oxide (GO) have been explored for applications as transparent electrodes in solar cells.[21−23] However, the devices obtained exhibited rather moderate performance, leakage current under dark conditions, and moderate power conversion efficiency of <0.4%. The moderate performance of these devices may be attributed to several factors, including the following: (i) reduction of oxygen functionalities on the graphene oxide flakes does not completely restore the π-conjugation in the films, and (ii) the

*Address correspondence to chongwuz@usc.edu.

Received for review November 10, 2009 and accepted April 02, 2010.

Published online April 15, 2010.
10.1021/nn901587x

vacuum filtration or spin-coating methods used to prepare reduced graphene oxide films lead to stacked graphene flakes and thus significant flake-to-flake resistance. For instance, Eda *et al.*[21] reported doped reduced graphene oxide films with a sheet resistance of 40 kΩ/sq, a transparency of 64%, and a solar cell conversion efficiency of 0.1%, while Wu *et al.*[23] reported reduced graphene oxide films of $5-10^3$ kΩ/sq, >80% transparency, and a conversion efficiency of 0.4%. Efforts to improve percolation on the graphene electrode include the use of reduced GO combined with carbon nanotube films, but this approach requires extra processing steps.[24] As a result, continuous, highly flexible, and transparent graphene films are still highly desirable for photovoltaic applications.

Chemical vapor deposition (CVD) has surged as an important method to obtain high-quality graphene films.[25−28] In particular, films with sheet resistance of 280 Ω/sq (80% transparent) and 770 Ω/sq (90% transparent) have been reported for graphene synthesized on Ni films, while sheet resistance of 350 Ω/sq (90% transparent) has been reported for CVD graphene on Cu films, which represents a good advance in the use of graphene as transparent conductive films. Another advantage of CVD is its scalability, and we have reported wafer-scale synthesis and transfer of single- and few-layer graphene for device fabrication.[25] In this work, we explore the implementation of large-area, smooth few-layer graphene films as the anode material in flexible and rigid OPV cells with multilayer structure, as shown in Figure 1a. Such films were synthesized by CVD and exhibit sheet resistance and transparency controlled in the range of 230 Ω/sq at 72% transparency and 8.3 kΩ/sq at 91% transparency. The use of CVD graphene is attractive, because other graphene films that are formed by stacked micrometer-sized flakes suffer from flake-to-flake contact resistance and high roughness. In contrast, grain boundaries of CVD graphene films have the advantage of being formed *in situ* during synthesis; such a process is expected to minimize contact resistance between neighboring graphene domains and may result in smoother films with better conducting properties. Solar cells made with CVD graphene exhibited performance that compares to ITO devices and surpasses that of ITO devices under bending conditions, exhibiting power conversion efficiencies of 1.18% and being operational under bending conditions up to 138°.

RESULTS AND DISCUSSION

Graphene Synthesis and Transfer. Graphene films were synthesized by chemical vapor deposition on a thermally annealed polycrystalline nickel surface composed mostly of the (111) plane (see Supporting Information). The graphene films were grown as detailed elsewhere.[25] This synthesis yields a continuous film comprising monolayer and few-layer graphene with low defect density, as indicated by TEM imaging and diffraction and micro-Raman spectroscopy measurements performed on the transferred films (see Supporting Information). After synthesis, graphene films were transferred to transparent substrates. A schematic illustrating the transfer process is shown in Figure 1b (a detailed description of the transfer process can be found in Methods). In brief, poly(methyl methacrylate) (PMMA) was deposited atop the as-synthesized graphene on $Si/SiO_2/Ni$ substrates, and etching of the nickel rendered free-standing PMMA with the synthesized graphene adhered to it, which facilitates transferring the graphene film to target substrates. Figure 1c,d shows photographs displaying see-through areas (dotted lines) of 2 and 1.3 cm^2 of graphene films after being transferred to glass and polyethylene terephthalate (PET), respectively. Thorough inspection of the graphene films using scanning electron microscopy confirmed the formation of continuous films without any visible cracks.

Characterization of CVD Graphene Film as Transparent Electrode for Organic Photovoltaics. The thin film nature of OPV devices requires control of layer thickness and morphology to reduce the possibility of leakage current and shorts.[22,23] Therefore, thickness and surface smoothness of the transparent electrode in OPVs are important for good device performance. As a point of reference, we compared the thickness and roughness given by CVD graphene films against single-walled carbon nanotubes (SWNTs) and ITO films, which are materials that have been amply reported in the literature as transparent electrodes.[29] The thickness of CVD graphene obtained at the above-mentioned synthesis conditions is on the order of 1−3 nm (see Supporting Information). In Figure 1f, AFM images of the CVD graphene, a commercial 150 nm thick ITO film (R_{sheet} = 20 Ω/sq), and a 30 nm thick SWNT film obtained by the filtration/PDMS transfer method (R_{sheet} = 1.1 kΩ/sq) are compared. The rms surface roughness measured for CVD graphene, ITO, and SWNT films was 0.9, 0.7, and 8.4 nm for graphene, ITO, and SWNT, respectively; such values were consistent with roughness previously reported for graphene,[22] ITO,[30] and SWNT[31] films. The obtained roughness values indicate that CVD graphene was nearly 10 times smoother and thinner than SWNT films, with surface roughness comparable to that of ITO. In addition, CVD graphene and SWNT films passivated with poly(3,4-ethylenedioxythiophene):poly(styrenesulfonate) (PEDOT:PSS) showed rms surface roughness of 0.8 and 5.1, respectively.

High transparency is also necessary for the use of CVD graphene as a substitute for transparent metal oxide electrodes in OPVs. Optical transmittance of the transferred graphene films in the visible and near-infrared range was measured using a Varian50 spectrophotometer in the wavelength range of 400−1100 nm. Figure 1e depicts the wavelength dependence of

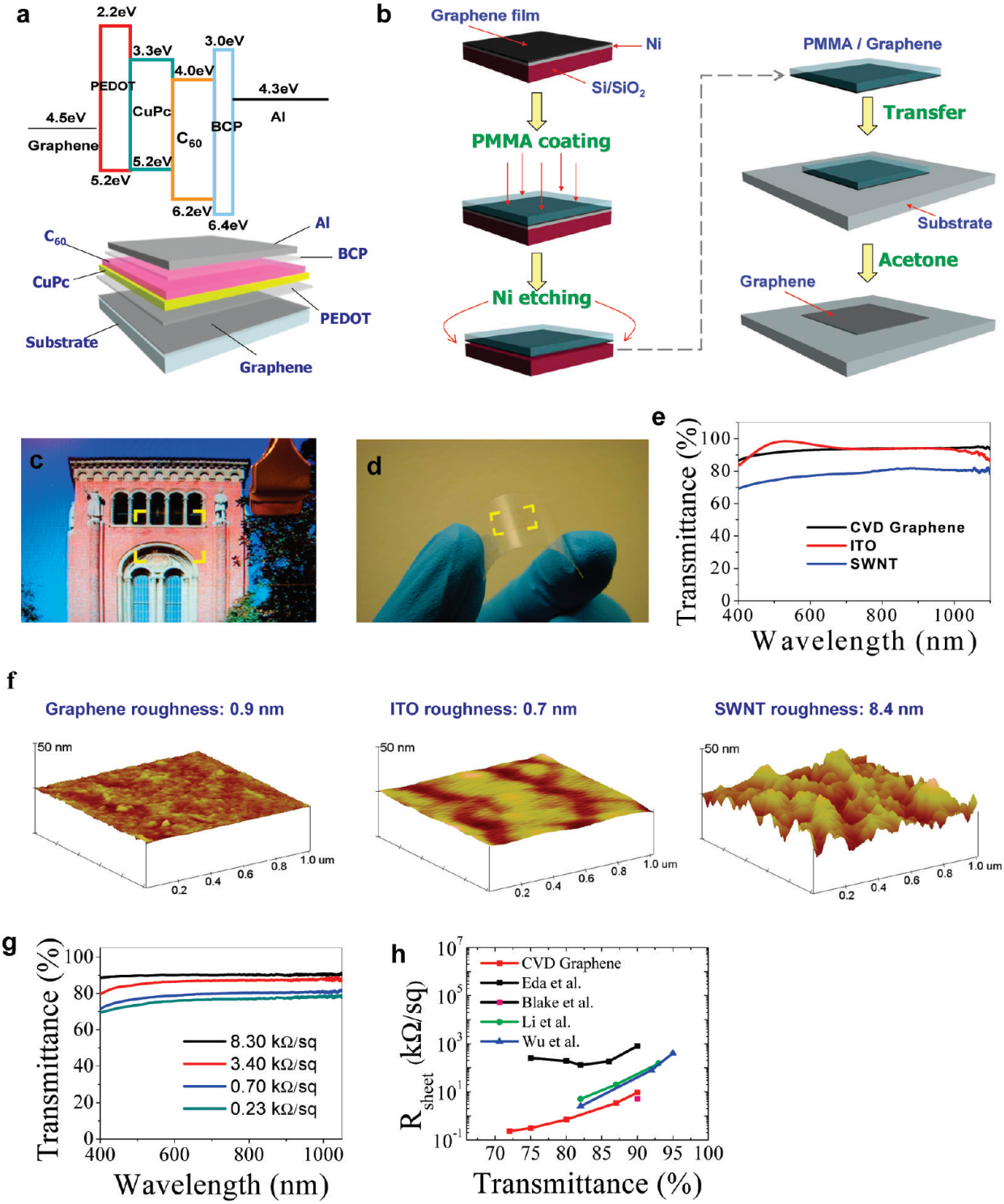

Figure 1. (a) Schematic representation of the energy level alignment (top) and construction of the heterojunction organic solar cell fabricated with graphene as anodic electrode: CVD graphene/PEDOT/CuPc/C_{60}/BCP/Al. (b) Schematic of the CVD graphene transfer process onto transparent substrates. Photographs showing highly transparent graphene films transferred onto glass and PET are shown in panels c and d, respectively. (e) Transmission spectra for CVD graphene, ITO, and SWNT films on glass. (f) AFM images of the surface of CVD graphene, ITO, and SWNT films on glass. The scale bar in *z*-direction is 50 nm for all images. (g) Transmission spectra of CVD graphene with different sheet resistance (R_{sheet}). (h) Comparison of R_{sheet} *vs* light transmittance at 550 nm for CVD graphene and reduced GO films reported in the literature.

the optical transparency of the CVD graphene, ITO, and SWNT films displayed in Figure 1f. For ITO films, the transmittance peaks at 535 nm, while the transmittance increases monotonically with the increase in wavelength of the incident light from $T = 86\%$ (at 400 nm) to $T = 95\%$ (at 1100 nm) and from $T = 70\%$ (at 400 nm) to $T = 82\%$ (at 1100) nm in graphene and SWNT films, respectively.

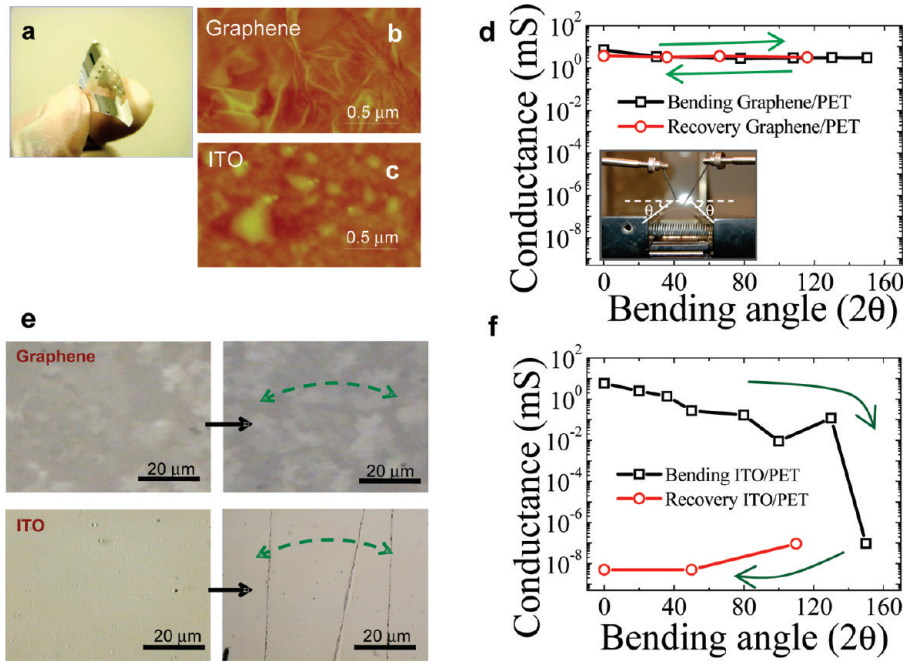

Figure 2. (a) Photograph illustrating high flexibility of CVD graphene transferred on a PET flexible substrate. (b,c) AFM images of the surface of CVD graphene and ITO films on PET, respectively. (d,f) Conductance of the CVD graphene and ITO films on PET substrates under bending conditions, respectively. The devices used to monitor the conductance had channel width (W) = 1 mm and length (L) = 1 mm. (e) Optical images of CVD graphene (top) and ITO (bottom) films on PET before and after being bent at the angles specified in panels b and c. Arrows show the direction of the bending.

Light transmission in graphene is dictated by absorption, due to the π-conjugated system. As a consequence of this, as CVD graphene films become thinner, transparency is expected to increase. In principle, the sheet resistance of a graphene film composed of several graphene layers should decrease for each layer added;[32] therefore, it is expected that the thicker the film, the larger the number of layers, the smaller the sheet resistance, but simultaneously, the lower the transparency. We were able to tune the transparency and sheet resistance of graphene films by varying the synthesis conditions. Figure 1g shows that highly transparent CVD graphene films can be obtained at the expense of higher resistance. Sheet resistance as low as 230 Ω/sq (with T = 72%) and optical transparency as high as 91% (with R_{sheet} = 8.3 kΩ/sq) can be achieved, and therefore, a compromise between these parameters must be met for specific applications. Further characterization of the CVD graphene films is shown in Figure 1h, where we compare sheet resistance and transparency of CVD graphene against reduced GO films reported in the literature. Analysis of Figure 1h shows that graphene synthesized by CVD exhibits better transparency/R_{sheet} ratio than the reduced graphene oxide films reported so far.[14,23,33,34] The transparency/R_{sheet} ratio of CVD graphene can be further improved to yield films with 700 Ω/sq and ~90% transparency.[27]

Flexible Transparent Electrodes: Graphene *versus* ITO. To investigate the flexibility of the CVD graphene electrodes and its influence on the performance of flexible OPV cells, we transferred CVD graphene films onto PET substrates (Figure 2a) and compared the electrical conductivity of graphene and ITO films under bending conditions. Figure 2b,c shows AFM images of CVD graphene (R_{sheet} = 500 Ω/sq and T = 75%) and ITO (R_{sheet} = 25 Ω/sq, T = 86%) on PET. The rms surface roughness of ITO on PET was 1.1 nm, nearly 60% higher than on glass (see Supporting Information). The 100 nm thick aluminum metal contacts were thermally deposited through a shadow mask onto the above-mentioned films. Two-probe electrical measurements were performed on both films by direct contact of tungsten microprobes to the aluminum electrodes, soldering the probe tips to the aluminum pads to ensure good electrical contact on each measurement. Performing this process for each bending angle allowed us to monitor the change in conductance of the film with the bending angle (inset Figure 2d). The conductance of the graphene/PET film remained virtually unperturbed by bending (Figure 2d) even after several complete bending cycles and decreased by only 7.9% after 100 bending cycles (see Supporting Information). In contrast, Figure 2f shows three clearly defined regions that describe the typical behavior of ITO conductance under bending conditions. For bending angles from 0 to ~130°, a steady decrease in the conductance of the ITO film by 3 orders of magnitude with increased bending angle was observed. Interestingly, immediately after a critical angle (128°), conductance suddenly fell by 6 orders of magnitude. Finally, after the critical angle was reached, the conductance of the film continued to decrease even when the bending angle decreases; an open circuit ($\sigma \leq 10^{-12}$ S)

was obtained after only one bending cycle. The fact that the conductivity of the ITO film did not recover after bending the ITO film back to lower radius of curvature can be associated with the development of multiple discontinuity scattering sites on the brittle ITO film that were generated by tensile strain under bending and may further develop under compressive stress while decreasing the bending angle. Optical microscopy images were collected on the ITO/PET and graphene/PET films. Figure 2e shows optical micrographs of graphene and ITO films before and after the first bending cycle (0° → 150° → 0°). As can be seen under the microscope resolution, very pronounced cracks were developed on the ITO film, while the graphene film remained intact. These results demonstrate the advantage of CVD graphene in terms of mechanical flexibility over ITO films, which opens new avenues for robust, flexible, and lightweight transparent CVD graphene electrodes in OPVs.

Graphene OPV Cell Fabrication on Flexible Substrate and Device Performance. Although CVD graphene films clearly outperform ITO as transparent conductive electrodes on flexible PET substrates under bending conditions, it is important to implement this material into working OPVs in order to evaluate its performance. Thus, we fabricated OPV cells on PET substrates using graphene and ITO as transparent electrodes, under identical experimental conditions. Graphene electrodes were fabricated by transferring as-grown CVD graphene films onto precleaned, 100 μm thick PET substrates. PET substrates coated with ITO were obtained from Southwall Technologies Inc. Both substrates were solvent cleaned and passivated by spin coating a thin layer (10 nm) of poly(3,4-ethylenedioxythiophene):poly(styrenesulfonate) with $R_{sheet} = 1$ kΩ/sq (PEDOT:PSS). Use of the PEDOT:PSS coating as the electron blocking layer decreased the conductivity of the PEDOT:PSS/CVD graphene film to 2.1 kΩ/sq, while for the PEDOT/ITO film, it remained ~1 kΩ/sq. PEDOT:PSS was expected to help mitigate the brittle nature of the ITO electrode to enhance its performance under bending conditions, and interestingly, PEDOT:PSS passivation of ITO was also found to improve the rectification behavior of the devices. Finally, the planarizing effect afforded by the PEDOT:PSS treatment is desirable to compensate for possible folding or wrinkles that may accompany the CVD graphene film transfer process or irregular wetting between the electrode and the cell active layers, which would yield device shorting or shunt losses.

The substrates were taken into high vacuum conditions where the organic thin films and the aluminum cathode were consecutively deposited by thermal evaporation. The multilayered configuration employed (Figure 1a) is given as CVD graphene [<5 nm] or ITO/PEDOT:PSS/copper phthalocyanine (CuPc) [40 nm]/fullerene (C_{60}) [40 nm]/bathocuproine (BCP) [10 nm]/aluminum (Al). Aluminum cathodes were deposited through a shadow mask with circular openings of 0.75 mm^2. Optical excitation of the CuPc (C_{60}) leads to the donation of an electron (hole) to C_{60} (CuPc), and the photogenerated charge carriers are swept to the external contacts, producing a measurable light-generated current.

Current density *versus* voltage or *J*(*V*) characteristics were measured in air at room temperature in the dark and under spectral mismatch corrected 100 mW/cm^2 white light illumination from an AM 1.5G filtered 300 W xenon arc lamp (Newport Co.). Routine spectral mismatch correction for ASTM G173-03 was performed using a filtered silicon photodiode calibrated by the National Renewable Energy Laboratory (NREL) to reduce measurement errors. Chopped monochromatic light (250 Hz, 10 nm fwhm) and lock-in detection were used to perform all spectral responsivity and spectral mismatch correction measurements.

We compared the *J*(*V*) characteristics of a typical photovoltaic cell obtained with CVD graphene ($R_{sheet} =$ 3.5 kΩ/sq, $T = 89\%$) against a typical cell obtained with an ITO anode ($R_{sheet} = 25$ Ω/sq, $T = 96\%$) that was fabricated under identical experimental conditions. Figure 3a,b shows semilog (top) and linear (bottom) *J*(*V*) plots obtained from CVD graphene and ITO OPV cells, respectively. Red and blue traces correspond to the current density measured in the dark and under illumination, respectively. The output power density of the cells (*P*), which is given by $P = JV$, is shown in Figure 3a,b as open circle traces for which the maximum point on the curve corresponds to the maximum output power density (P_{max}) of the device. For an incident power density, $P_{inc} = 100$ mW/cm^2, the power conversion efficiency ($\eta = P_{max}/P_{inc}$) and other performance parameters are summarized in Table 1. It is clearly observed from the semilog plots in Figure 3a,b that both devices have nearly identical open-circuit voltage (V_{oc}) (for $J = 0$) of 0.48 V under illumination conditions, which suggests similar recombination behavior in both cells. Furthermore, from Figure 3a, it can be seen that, unlike OPVs reported for reduced GO anodes,[23,24] we did not observe large leakage current densities from any of the CVD graphene OPV cells.

The *J*(*V*) characteristics of the CVD graphene cell under illumination showed a short-circuit photocurrent density (J_{sc}) (for $V = 0$) of 4.73 mA/cm^2, an open-circuit voltage (V_{oc}) of 0.48 V, and a maximum power (P_{max}) of 1.18 mW/cm^2 to yield a fill factor (FF) of 0.52 and overall power conversion efficiency (η) of 1.18%. The control device, using an ITO anode on PET, gave J_{sc} of 4.69 mA/cm^2, V_{oc} of 0.48 V, and P_{max} of 1.27 mW/cm^2 for a FF of 0.57 and an efficiency of 1.27%. Analysis of Figure 3a,b reveals that, despite the lower transparency and higher R_{sheet} of the CVD graphene electrode, CVD graphene solar cell exhibits an output power density nearly 93% of that shown by the ITO device. We also observed that CVD graphene OPV cells were more sensitive to the an-

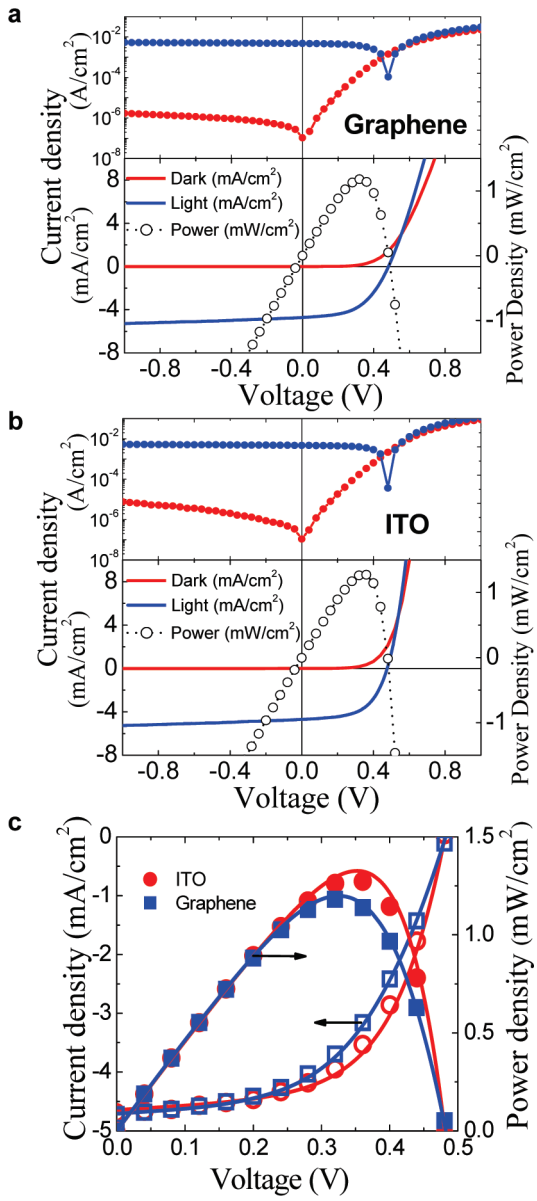

Figure 3. Logarithmic (top) and linear (bottom) current density and power density *vs* voltage characteristics of CVD graphene (a) and ITO (b) OPV cells on PET under dark (red traces) and 100 mW/cm² AM1.5G spectral illumination (blue traces). The output power density of the cells is plotted in panels a and b as open circle traces. The structure of the devices is given by [CVD graphene/PEDOT/CuPc/C_{60}/BCP/Al] and [ITO/CuPc/C_{60}/BCP/Al] for CVD graphene and ITO OPVs, respectively. (c) Comparison of the modeled (solid lines) current density and power density curves of the graphene and ITO devices obtained from the Shockley equation against the experimentally (dots) obtained values.

ode conductivity and, hence, to its capacity to pull holes from the active layers than to its transparency.

TABLE 1. Performance Details of OPV Cells Built on PET[a]

anode	J_{sc} (mA/cm²)	V_{oc} (V)	FF	η (%)
CVD graphene	4.73	0.48	0.52	1.18
ITO	4.69	0.48	0.57	1.27

[a]The structure of the devices is given by [CVD graphene/PEDOT/CuPc/C_{60}/BCP/Al] and ITO/PEDOT/CuPc/C_{60}/BCP/Al] for CVD graphene and ITO OPVs, respectively.

The fact that the two cells gave very similar device performance is encouraging, especially considering that the ITO substrate gave ~100-fold lower R_{sheet} and higher transparency than the CVD graphene film, which would favor the performance of the ITO device.[35] This may be rationalized by considering that, as demonstrated above, the sheet resistance increases to similar values on both electrodes after being coated with PEDOT:PSS. In this case, charge injection from the active layers of the OPV cells may be limited by the PEDOT:PSS layer, thus yielding similar performance on both cells. We fabricated OPV cells on PET/PEDOT:PSS substrates without graphene or ITO, and all of them produced open-circuit characteristics. Although PEDOT:PSS was used on both graphene and ITO OPV cells, the performance of the cells was measured by puncturing the PEDOT:PSS layer to contact the underlying electrode material, which confirms that CVD graphene and ITO anodes, instead of PEDOT:PSS, are the ultimate electrodes in the hole extraction process of the devices.

Device Performance Model: The Lamber-W Function. To estimate the impact of resistive losses on device performance, the $J(V)$ dependence under illumination was modeled according to a modified form of the Shockley equation, which is commonly applied to describe the current density (J) *versus* voltage (V) characteristics of organic solar cells, given by

$$J = J_s\left\{\exp\left(\frac{V - JR_s}{nV_t}\right) - 1\right\} + \frac{V - JR_s}{R_p} - J_{ph} \quad (1)$$

where R_s, R_p, J_s, J_{ph}, n, and V_t are the lumped series resistance, lumped parallel resistance, reverse-bias saturation current density, photocurrent density, diode ideality factor, and thermal voltage, respectively, for a single diode circuit model. As a practical matter, the transcendental nature of eq 1 was resolved by expressing it in terms of the Lambert-W function[36] (see Supporting Information) to give

$$J = \frac{nV_t}{R_s}W_0\left\{\frac{J_sR_sR_p}{nV_t(R_s + R_p)}\exp\left(\frac{R_p}{nV_t}\frac{V + R_s(J_{ph} + J_s)}{(R_s + R_p)}\right)\right\} - \frac{R_p(J_{ph} + J_s) - V}{(R_s + R_p)} \quad (2)$$

where W_0 represents Lambert's function of the form $W(x)e^{W(x)} = x(V)$.[36−39]

In Figure 3c, the modeled $J(V)$ and output power density obtained according to eq 2 are plotted as solid lines for the CVD graphene and ITO cells depicted in Figure 3a,b, respectively. The modeled data are compared against the experimentally measured values, plotted as open symbols in Figure 3c, demonstrating that these CVD graphene-based devices may be described by the generalized Shockley equation in the same way that their ITO-based counterparts are commonly discussed. Modeling the data in this way allows us to estimate to what extent series resistive losses,

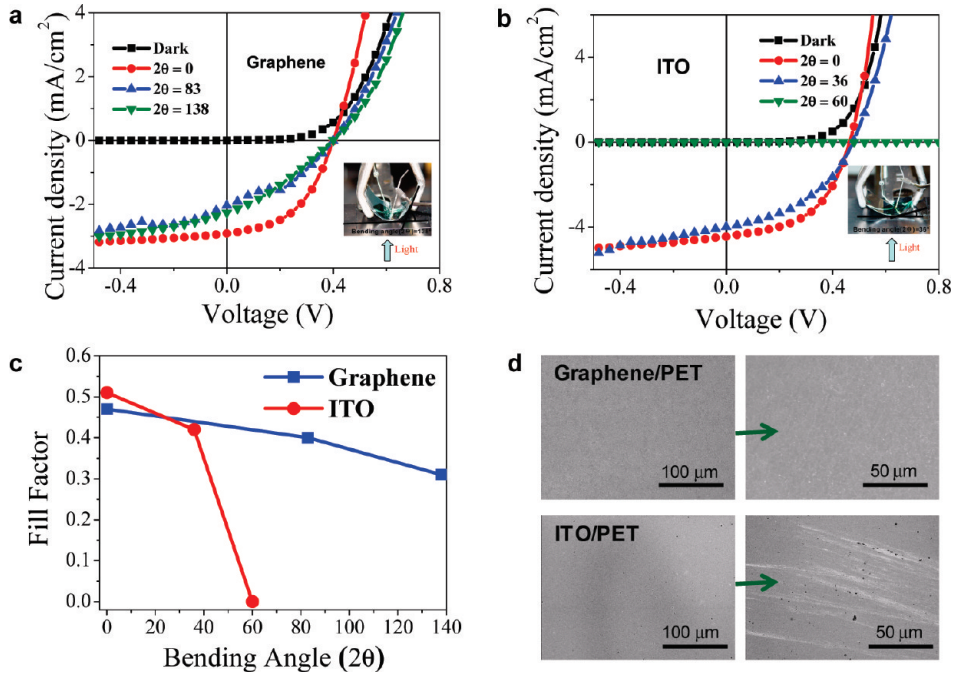

Figure 4. Current density *vs* voltage characteristics of CVD graphene (a) or ITO (b) photovoltaic cells under 100 mW/cm^2 AM1.5G spectral illumination for different bending angles. Insets show the experimental setup employed in the experiments. (c) Fill factor dependence of the bending angle for CVD graphene and ITO devices. (d) SEM images showing the surface structure of CVD graphene (top) and ITO (bottom) photovoltaic cells after being subjected to the bending angles described in panels a and b.

parallel conductance, and recombination processes may impact device performance. The model ideality factors, parallel resistances, and saturation current densities were all comparable for the ITO and CVD graphene devices under illumination, having values of $n = 2.4$ and 2.6, $R_p = 1.47$ and 1.62 kΩ cm^2, and $J_s = 2.0$ and 3.1 μA/cm^2, respectively, suggesting that the recombination and leakage processes are similar for both devices. The model series resistance calculated from eq 2 for the CVD graphene device is 12.6 Ωcm^2, which is less than 5 times that of the ITO device with $R_s = 2.6$ Ω cm^2, while the model photocurrent density (J_{ph}) for the CVD graphene device (4.75 mA/cm^2) is higher than J_{ph} for the ITO device (4.66 mA/cm^2). This indicates that the power output of the graphene-based device is primarily limited by charge transport losses rather than optical transmittance losses. This constitutes a very promising result for CVD graphene transparent electrodes, which perform comparably to ITO, despite carrying a relatively higher sheet resistance.

Performance of Highly Flexible Graphene OPV Cell under Bending. Given the good performance of OPVs with graphene electrodes, the question remains if such devices will perform well under strain−stress conditions. Current−voltage characteristics under bending of CVD graphene and ITO solar cells are shown in Figure 4a,b, respectively. We observed that the performance of both devices was slightly degraded upon bending. For instance, solar cells using CVD graphene electrodes withstood bending angles (curvature radii, surface strain) up to 138° (4.1 mm, 2.4%) while exhibiting good solar cell performance. In sharp contrast, ITO cells only withstood bending to 36° (15.9 mm, 0.8%) while showing poor performance and failed completely to become an open circuit after being bent to 60° (9.5 mm, 1%).

It is important to note that, with increased bending angle, the current density dropped for CVD graphene and ITO devices, while their open-circuit voltage remained virtually unchanged. In some cases, this effect can be associated with decreased illumination of the devices during bending. However, as both cells are subjected to similar bending conditions, the marked difference exhibited in the conversion efficiency between them cannot be attributed to irregular illumination induced by bending, but may be related to the presence of microcracks on the ITO device. To further investigate this, we plotted the fill factor *versus* the bending angle of the OPV cells with CVD graphene and ITO electrodes (Figure 4c). The fill factor (FF = $P_{max}/J_{sc}V_{oc}$) depends strongly on the output power of the cell and is directly related to the cell conversion efficiency (η) by

$$\eta = \mathrm{FF}\frac{J_{sc}V_{oc}}{P_{inc}} \times 100 \qquad (3)$$

Gradual degradation of the initial fill factor and, hence, the conversion efficiency was observed on the CVD graphene cell as the bending angle increased; in contrast, the fill factor of the ITO device rapidly decayed to 0 when bent at around 60°. Furthermore, we performed SEM measurements to investigate changes in film morphology that may have been introduced by bending

of the devices. Figure 4d shows the appearance of microcracks throughout the ITO device, while no signs of microcracks or fissures were observed on the graphene device. Development of microcracks generated by mechanical stress in ITO, even at small bending angles, can substantially increase the film resistance, which has a key impact in reducing the fill factor. This agrees well with the observed decrease in output current density and power conversion efficiency of the solar cells without observing appreciable change in the V_{oc}. CVD graphene, being of organic nature and more flexible, surpasses the performance of ITO, which may easily crack under slight bending albeit PEDOT:PSS passivation. Therefore, the brittle nature of ITO plays a major role in the resulting poor performance of ITO-flexible organic solar cells, while the CVD graphene thin films exhibited good performance as flexible transparent electrodes. OPVs based on CVD graphene transferred to glass were also made, and details can be found in the Supporting Information.

CONCLUSIONS

In summary, this work demonstrates a feasible, scalable, and effective method to employ CVD graphene as highly transparent, continuous, and flexible electrodes for OPVs. This approach constitutes a significant advance toward the production of transparent conductive electrodes in solar cells. CVD graphene meets the most important criteria of abundance, low cost, conductivity, stability, electrode/organic film compatibility, and flexibility that are necessary to replace ITO in organic photovoltaics, which may have important implications for future organic optoelectronic devices.

METHODS

CVD Graphene Synthesis. Elemental Ni was thermally evaporated onto precleaned Si/SiO_2 substrates up to a thickness of ~1000 Å. Subsequently, $Ni/Si/SiO_2$ substrates were taken into a sealed high-temperature furnace and heated to 900 °C under a hydrogen flow rate of 600 sccm. Graphene synthesis was obtained at 900 °C by flowing methane at a flow rate of 100 sccm for 8 min.

CVD Graphene Transfer. CVD graphene was transferred by depositing a thin layer (300 nm) of poly(methyl methacrylate) (PMMA) on top of the as-synthesized graphene on $Si/SiO_2/Ni$ substrates by spin coating. Nickel underneath the graphene was dissolved by dipping the substrates in aqueous nitric acid solution (14% w/w) for approximately 1 h under constant heating at 90 °C or until the Ni film was etched to levels below the limit of detection of an Omicron XPS/UPS system (<0.1−1 atom %). PMMA/graphene was transferred by direct graphene contact onto transparent substrates such as glass and polyethylene terephthalate (PET) sheets. Then, the PMMA layer was finally dissolved with acetone for ~10 min, leaving the graphene film on the target substrate surface.

Organic Photovoltaic Cell Fabrication with CVD Graphene and ITO. Graphene electrodes were fabricated by transferring as-grown CVD graphene films onto precleaned PET substrates. PET substrates coated with ITO were obtained from Southwall Technologies Inc. Both substrates were solvent cleaned and passivated by spin coating a thin layer of poly(3,4-ethylenedioxythiophene): poly(styrenesulfonate) (PEDOT:PSS). Organic thin films and the aluminum cathode were consecutively deposited by thermal evaporation to form a multilayered configuration: CVD graphene or ITO/PEDOT:PSS/copper phthalocyanine (CuPc)/fullerene (C_{60})/bathocuproine (BCP)/aluminum (Al). Aluminum cathodes were deposited through a shadow mask with circular openings of 0.75 mm^2.

Acknowledgment. This work was supported by the National Science Foundation under Grant CCF-0702204, by the Center for Advanced Molecular Photovoltaics (CAMP) (KUS-C1-015-21), made by King Abdullah University of Science and Technology (KAUST), and by Global Photonic Energy Corporation.

Supporting Information Available: Additional information can be found describing X-ray diffraction of Ni substrates, TEM, SAED, AFM, and Raman characterization of the synthesized graphene films. Information regarding the fabrication and performance of CVD graphene organic photovoltaic cells on rigid substrates, model for device parameter extraction of CVD graphene, and ITO-based OPVs and conductance *vs* bending cycles of flexible CVD graphene films is also included. This material is available free of charge *via* the Internet at http://pubs.acs.org.

REFERENCES AND NOTES

1. Peumans, P.; Yakimov, A.; Forrest, S. R. Small Molecular Weight Organic Thin-Film Photodetectors and Solar Cells. *J. Appl. Phys.* **2003**, *93*, 3693–3723.
2. Andersson, A.; Johansson, N.; Bröms, P.; Yu, N.; Lupo, D.; Salaneck, W. R. Fluorine Tin Oxide as an Alternative to Indium Tin Oxide in Polymer LEDs. *Adv. Mater.* **1998**, *10*, 859–863.
3. Jansseune, T. Indium Price Soars as Demand for Displays Continues to Grow. *Comp. Semicond.* **2005**, *11*, 34–35.
4. Scott, J. C.; Kaufman, J. H.; Brock, P. J.; DiPietro, R.; Salem, J.; Goitia, J. A. Degradation and Failure of MEH-PPV Light-Emitting Diodes. *J. Appl. Phys.* **1996**, *79*, 2745–2751.
5. Boehme, M.; Charton, C. Properties of ITO on PET Film in Dependence on the Coating Conditions and Thermal Processing. *Surf. Coat. Technol.* **2005**, *200*, 932–935.
6. Wu, Z.; Chen, Z.; Du, X.; Logan, J. M.; Sippel, J.; Nikolou, M.; Kamaras, K.; Reynolds, J. R.; Tanner, D. B.; Hebard, A. F.; Rinzler, A. G. Transparent, Conductive Carbon Nanotube Films. *Science* **2004**, *305*, 1273–1276.
7. Barnes, T. M.; X. Wu, J. Z.; Duda, A.; Lagemaat, J. v. d.; Coutts, T. J.; Weeks, C. L.; Britz, D. A.; Glatkowski, P. Single-Wall Carbon Nanotube Networks as a Transparent Back Contact in CdTe Solar Cells. *Appl. Phys. Lett.* **2007**, *90*, 243503.1243503.3.
8. Rowell, M. W.; Topinka, M. A.; McGehee, M. D.; Prall, H.-J.; Dennler, G.; Sariciftci, N. S.; Hu, L.; Gruner, G. Organic Solar Cells with Carbon Nanotube Network Electrodes. *Appl. Phys. Lett.* **2006**, *88*, 233506.1233506.3.
9. Kang, M.-G.; Guo, L. J. Nanoimprinted Semitransparent Metal Electrodes and Their Application in Organic Light-Emitting Diodes. *Adv. Mater.* **2007**, *19*, 1391–1396.
10. Lee, J.-Y.; Connor, S. T.; Cui, Y.; Peumans, P. Solution-Processed Metal Nanowire Mesh Transparent Electrodes. *Nano Lett.* **2008**, *8*, 689–692.
11. Zhang, Y.; Tan, Y.-W.; Stormer, H. L.; Kim, P. Experimental Observation of the Quantum Hall Effect and Berry's Phase in Graphene. *Nature* **2005**, *438*, 201–204.
12. Nair, R. R.; Blake, P.; Grigorenko, A. N.; Novoselov, K. S.; Booth, T. J.; Stauber, T.; Peres, N. M. R.; Geim, A. K. Fine Structure Constant Defines Visual Transparency of Graphene. *Science* **2008**, *320*, 1308.
13. Geim, A. K.; Novoselov, K. S. The Rise of Graphene. *Nat. Mater.* **2007**, *6*, 183–191.
14. Blake, P.; Brimicombe, P. D.; Nair, R. R.; Booth, T. J.; Jiang, D.; Schedin, F.; Ponomarenko, L. A.; Morozov, S. V.; Gleeson, H. F.; Hill, E. W.; Geim, A. K.; Novoselov, K. S. Graphene-Based Liquid Crystal Device. *Nano Lett.* **2008**, *8*, 1704–1708.

15. Tan, Y. W.; Zhang, Y.; Bolotin, K.; Zhao, Y.; Adam, S.; Hwang, E. H.; Das Sarma, S.; Stormer, H. L.; Kim, P. Measurement of Scattering Rate and Minimum Conductivity in Graphene. *Phys. Rev. Lett.* **2007**, *99*, 246803.1246803.4.
16. Echtermeyer, T. J.; Lemme, M. C.; Bolten, J.; Baus, M.; Ramsteiner, M.; Kurz, H. Graphene Field-Effect Devices. *Eur. Phys. J (Special Topic)* **2007**, *148*, 19–26.
17. Forbeaux, I.; Themlin, J.-M.; Debever, J.-M. Heteroepitaxial Graphite on 6h-Sic(0001): Interface Formation through Conduction-Band Electronic Structure. *Phys. Rev. B* **1998**, *58*, 16396–16406.
18. Novoselov, K. S.; Geim, A. K.; Morozov, S. V.; Jiang, D.; Zhang, Y.; Dubonos, S. V.; Grigorieva, I. V.; Firsov, A. A. Electric Field Effect in Atomically Thin Carbon Films. *Science* **2004**, *306*, 666–669.
19. Viculis, L. M.; Mack, J. J.; Kaner, R. B. A Chemical Route to Carbon Nanoscrolls. *Science* **2003**, *299*, 1361.
20. Gilje, S.; Han, S.; Wang, M.; Wang, K. L.; Kaner, R. B. A Chemical Route to Graphene for Device Applications. *Nano Lett.* **2007**, *7*, 3394–3398.
21. Eda, G.; Lin, Y.-Y.; Miller, S.; Chen, C.-W.; Su, W.-F.; Chhowalla, M. Transparent and Conducting Electrodes for Organic Electronics from Reduced Graphene Oxide. *Appl. Phys. Lett.* **2008**, *92*, 233305.1233305.3.
22. Wang, X.; Zhi, L.; Müllen, K. Transparent, Conductive Graphene Electrodes for Dye-Sensitized Solar Cells. *Nano Lett.* **2008**, *8*, 323–327.
23. Wu, J.; Becerril, H. A.; Bao, Z.; Liu, Z.; Chen, Y.; Peumans, P. Organic Solar Cells with Solution-Processed Graphene Transparent Electrodes. *Appl. Phys. Lett.* **2008**, *92*, 263302.1263302.3.
24. Tung, V. C.; Chen, L.-M.; Allen, M. J.; Wassei, J. K.; Nelson, K.; Kaner, R. B.; Yang, Y. Low-Temperature Solution Processing of Graphene−Carbon Nanotube Hybrid Materials for High-Performance Transparent Conductors. *Nano Lett.* **2009**, *9*, 1949–1955.
25. Gomez, L.; Zhang, Y.; Kumar, A.; Zhou, C. Synthesis, Transfer and Devices of Single- and Few-Layer Graphene by Chemical Vapor Deposition. *IEEE Trans. Nanotechnol.* **2009**, *8*, 135–138.
26. Yu, Q.; Lian, J.; Siriponglert, S.; Li, H.; Chen, Y. P.; Pei, S.-S. Graphene Segregated on Ni Surfaces and Transferred to Insulators. *Appl. Phys. Lett.* **2008**, *93*, 113103.1113103.3.
27. Reina, A.; Jia, X.; Ho, J.; Nezich, D.; Son, H.; Bulovic, V.; Dresselhaus, M. S.; Kong, J. Large Area, Few-Layer Graphene Films on Arbitrary Substrates by Chemical Vapor Deposition. *Nano Lett.* **2008**, *9*, 30–35.
28. Kim, K. S.; Zhao, Y.; Jang, H.; Lee, S. Y.; Kim, J. M.; Kim, K. S.; Ahn, J.-H.; Kim, P.; Choi, J.-Y.; Hong, B. H. Large-Scale Pattern Growth of Graphene Films for Stretchable Transparent Electrodes. *Nature* **2009**, *457*, 706–710.
29. Sangeeth, C. S. S.; Manu, J.; Reghu, M. Charge Transport in Transparent Conductors: A Comparison. *J. Appl. Phys.* **2009**, *105*, 063713.1063713.6.
30. Kim, K.-B.; Tak, Y.-H.; Han, Y.-S.; Baik, K.-H.; Yoon, M.-H.; Lee, M.-H. Relationship between Surface Roughness of Indium Tin Oxide and Leakage Current of Organic Light-Emitting Diode. *Jpn. J. Appl. Phys.* **2003**, *42*, L438–L440.
31. Zhang, D.; Ryu, K.; Liu, X.; Polikarpov, E.; Ly, J.; Tompson, M. E.; Zhou, C. Transparent, Conductive, and Flexible Carbon Nanotube Films and Their Application in Organic Light-Emitting Diodes. *Nano Lett.* **2006**, *6*, 1880–1886.
32. Li, X.; Zhu, Y.; Cai, W.; Borysiak, M.; Han, B.; Chen, D.; Piner, R. D.; Colombo, L.; Ruoff, R. S. Transfer of Large-Area Graphene Films for High-Performance Transparent Conductive Electrodes. *Nano Lett.* **2009**, *9*, 4359–4363.
33. Eda, G.; Fanchini, G.; Chhowalla, M. Large-Area Ultrathin Films of Reduced Graphene Oxide as a Transparent and Flexible Electronic Material. *Nat. Nanotechnol.* **2008**, *3*, 270–274.
34. Li, X.; Zhang, G.; Bai, X.; Sun, X.; Wang, X.; Wang, E.; Dai, H. Highly Conducting Graphene Sheets and Langmuir−Blodgett Films. *Nat. Nanotechnol.* **2008**, *3*, 538–542.
35. Wang, X.; Zhi, L.; Tsao, N.; Tomović, Ž.; Li, J.; Müllen, K. Transparent Carbon Films as Electrodes in Organic Solar Cells. *Angew. Chem., Int. Ed.* **2008**, *47*, 2990–2992.
36. Hayes, B. Why W? *Am. Sci.* **2005**, *93*, 104–108.
37. Banwell, T. C.; Jayakumar, A. Exact Analytical Solution for Current Flow through Diode with Series Resistance. *Electron. Lett.* **2000**, *36*, 291–292.
38. Jain, A.; Kapoor, A. Exact Analytical Solutions of the Parameters of Real Solar Cells Using Lambert W-Function. *Sol. Energy Mater. Sol. Cells* **2004**, *81*, 269–277.
39. Ortiz-Conde, A.; García Sánchez, F. J.; Muci, J. Exact Analytical Solutions of the Forward Non-ideal Diode Equation with Series and Shunt Parasitic Resistances. *Solid-State Electron.* **2000**, *44*, 1861–1864.